Opening rates of DNA hairpins: Experiment and model

Jeungphill Hanne and Giovanni Zocchi
Department of Physics and Astronomy, University of California Los Angeles, Los Angeles, California 90095-1547, USA

Nikolaos K. Voulgarakis, Alan R. Bishop, and Kim Ø. Rasmussen
Center for Nonlinear Studies and Theoretical Division, Los Alamos National Laboratory, Los Alamos, New Mexico 87545, USA

(Received 22 August 2006; revised manuscript received 7 March 2007; published 16 July 2007)

We present single-molecule measurements of the opening rate of DNA hairpins under mechanical tension and compare with the results obtained from a reduced-degrees-of-freedom statistical mechanics model. We extract the apparent position of the transition state s and find that the model, with no fitting parameters, reproduces the experimental measurements surprisingly well. Our values for s are different from the ones obtained in previous experiments, where, however, the experimental conditions were different (different force fields, different salt concentrations). Thus it appears that the values of s measured for relatively short hairpins are strongly affected by these experimental conditions.

DOI: 10.1103/PhysRevE.76.011909 PACS number(s): 87.15.He

I. INTRODUCTION

Biomolecular interactions are often characterized by extended molecular surfaces interacting through many weak bonds; examples are the formation of protein, RNA, and DNA secondary structure, and protein-DNA complexes. Some features of the corresponding spatially extended energy landscapes can be revealed by dynamic force spectroscopy [1]. In addition, the force dependence of the rates provides insight into the dynamics of conformational changes. Studies were conducted, for example, on receptor-ligand interactions [1,2], protein-DNA interactions [3,4], the unraveling rate of RNA [5,6], and DNA [7–11] secondary structure. The kinetics of DNA secondary structure formation in particular has long attracted the interest of researchers [12–16]. Here we report single-molecule measurements of the opening rate of DNA hairpins under mechanical stress, exploiting a relatively simple experimental setup which we have previously used to study the dynamics of protein-DNA binding [4]. Our experiment differs from previous studies of hairpins in several respects: the force field is nonhomogeneous in space on the scale of the hairpin, the ends of the DNA hairpin are coupled to the solid surfaces through very short ($\sim$5 nm) arms, and the salt conditions are different. We analyze the force dependence of the opening rate in the canonical way [17]: from the slope of the plot of the logarithm of the rate versus force one extracts a length scale s which, in a two-state description, is the apparent position of the transition state in the direction of the applied force. For our hairpins with stem length 10 bp, at pH=7.4 and 50 mM monovalent salt, we find $s \approx 0.5-1$ nm.

Previous experiments on DNA hairpins with stems of comparable lengths (10–15 bp) found larger values for s [10,11]. However, these experiments were performed under different conditions. A comprehensive study [11] was performed at constant force and in 200 mM salt; they found that s increases linearly with stem length and, more specifically, $s \approx 5$ nm for a stem length of 10 bp. The earlier study [10] was at constant pulling rate and 100 mM salt; for a stem of 15 bp, they found $s \approx 1.9$ nm.

In an effort to understand which factors in the different experiments affect the determination of s, we use the well-established Peyrard-Bishop-Dauxois (PBD) model of DNA melting to simulate the experiments. This is interesting because changing parameters in the experiments is tedious and often it is not possible to change only one parameter at a time, whereas in the model this is accomplished relatively easily. The PBD model [18] is a reduced-degrees-of-freedom statistical mechanics description where the main parameters are the strength of the base-pairing potential, the strength of the base-stacking potential, and the strength of the coupling between pairing and stacking; it has been previously shown that this model not only successfully reproduces details of the thermal denaturation transition of double-stranded DNA [19,20], but it can also, through the use of Monte Carlo simulations, provide significant insight into the mechanical unzipping of double-stranded DNA [21]. Here we use the PBD model with the same parameter values which were used before to reproduce the equilibrium melting curves of DNA oligomers [19,20]; we simulate constant force pulling using the sequences of the present experiment and extract s in the same way as in the experiments, obtaining $s \approx 0.6$ nm. Thus, with no refitting of the model parameters, we obtain a surprisingly good agreement in the dynamics between the model and the present experiments.

Next we examine the question of relating constant force and constant pulling rate experiments, which is in general delicate. It has been pointed out previously [22] that even for a single-barrier energy landscape, the canonical analysis for constant force and constant rate [23,24] are generally not equivalent, and alternative approaches have been proposed [22,25]. A recent study [6] of an RNA hairpin where both constant force and constant rate measurements are obtained from the same experimental setup finds, however, comparable results for the two methods. We examine this question with the PBD model, performing constant-force and constant-rate simulations for the same sequence: namely, the 15-bp-long sequence of [10]. We find two different values for s in the two cases, $s \approx 0.56$ nm and $s \approx 1.2$ nm, respectively. Thus the model argues that constant-force and constant-rate experiments are in fact not equivalent.

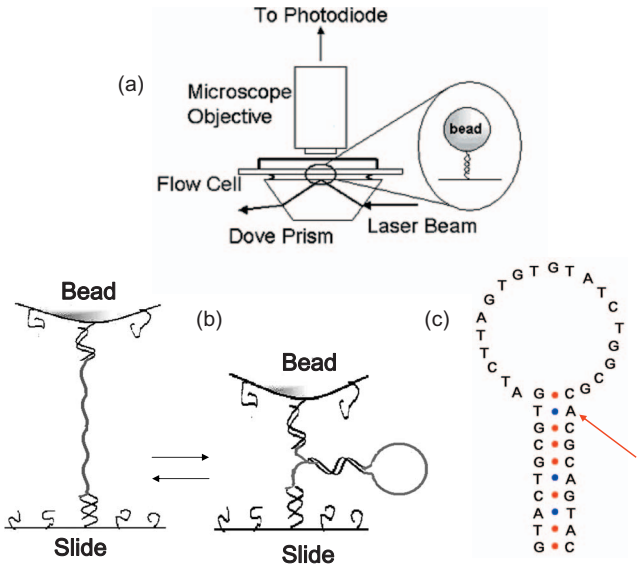

FIG. 1. (Color online) Experimental setup. (a) Evanescent-wave scattering optics. (b) The 1-μm-diam bead is tethered to the slide by a single 74-bases-long ssDNA molecule containing the 40-bases DNA hairpin. The average position of the bead moves up and down as the hairpin opens and closes. (c) One DNA hairpin investigated, H_{AT}, is 40 bases long, with a stem length of 10 bp, and a 20-bases-long loop. The second hairpin in this study (H_{GC}) differs only by the substitution AT$\rightarrow$GC (arrow).

In summary, the present study, when compared with the previous work [10,11], argues that for relatively short stems ($\sim$10 bp) the apparent position of the transition state as measured by the parameter s is dependent on the detailed conditions of the experiment: the properties of the force field, the base sequence, and the salt conditions. On the negative side, we were not able to pinpoint more precisely the origin of the differences in the measured values of s between the three experiments which we are comparing (the present one, [10], and [11]). On the constructive side, we contribute new measurements of hairpin dynamics and show that the PBD model describes this dynamics fairly well. The conditions of the experiment (a force field which is nonuniform on the scale of the hairpin) are possibly more relevant to what happens in the cell, where DNA is mechanically opened by enzymes, compared to constant-force or constant-pulling-rate experiments.

II. RESULTS

A. Experimental measurements

We report measurements on two DNA hairpins, both with a 10 bp-long stem and 20-bases-long loop (Fig. 1), differing by 1 bp (AT$\rightarrow$GC) in the stem. In the experiments we measure the relation between the external force field acting on the hairpin and its opening dynamics. The probe is a 1-μm-diam bead tethered to the surface of a microscope slide through a single 74-bases-long DNA construct which contains the hairpin (Fig. 1). We have shown previously that by monitoring the position of the bead relative to the surface

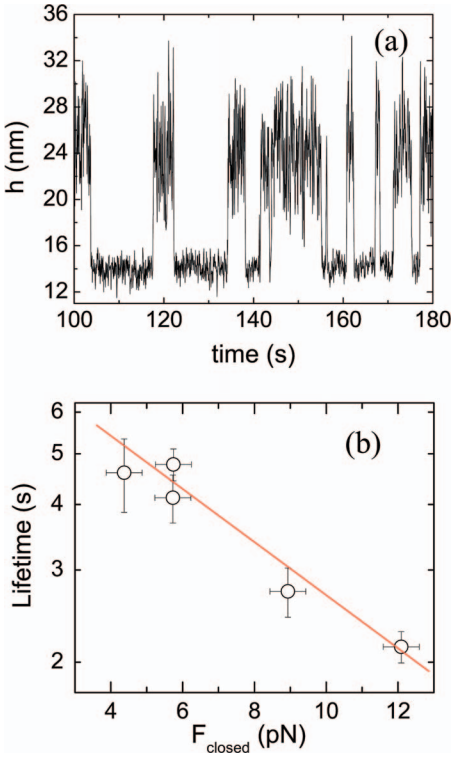

FIG. 2. (Color online) (a) Part of a time series of the bead's position with respect to the slide, showing the DNA hairpin tether repeatedly switching from the open (larger h) to the closed (smaller h) state. For each event we measure the duration of the closed state, Δ. The interaction potential corresponding to this time series is shown in Fig. 3(b). For this sample, $F_{closed} \approx 8.9$ pN. (b) Semilogarithmic plots of the opening rate vs the force in the closed state, $F_{closed} = (d\phi/dx)$ $(x = x_c)$, for the hairpin H_{AT}. The slope of the linear fit defines a characteristic length scale (the distance from the closed state to the transition state) $s \approx 0.42 \pm 0.06$ nm, and the intercept defines the extrapolated zero-force opening rate $r(0) \approx (1.36 \pm 0.20) \times 10^{-1}$ s^{-1}. Vertical error bars represent the statistical error ($\pm 1/2$ SD) from the finite sample size (determined by a simulation [4]). Horizontal error bars mainly represent the resolution in determining the position of the closed state on the time traces.

we can detect conformational changes in the molecular tether [26]. The bead's position is monitored optically by evanescent-wave scattering [27]. Analyzing the thermal motion of the bead we determine the force field acting on the tether [28]. The bead is in a nonhomogeneous field of force due to the electrostatic and entropic repulsion between bead and slide caused by the charged polymers grafted on the surfaces [see Fig. 1(b)] and the restoring force of the molecular tether. While in this setup we cannot set the force field externally, different realizations of the experiment give rise to different force fields (depending on the detailed surface topography around the tether), which we can measure.

A typical time trace from a hairpin-tethered bead is shown in Fig. 2(a): the system jumps between two states, corresponding to the closed and open conformations of the hairpin. The difference in average bead-slide separation between the two states [$\Delta h \approx 11$ nm in Fig. 2(a)] is consistent with the stem and loop length of the DNA hairpin, which is a total of 40 bases. From these recordings we measure the duration of

the closed states, obtain the corresponding cumulative distribution [an example is shown in Fig. 3(a)] and thus the lifetime of the closed state. In Fig. 3(b) we show a measured bead-slide interaction potential constructed from the Brownian motion of the bead in the open state. The derivative of this potential at the position x_c corresponding to the closed state gives the tension on the tether in the closed state [4,26–28]: $F_{\text{closed}}=(d\phi/dx)(x=x_c)$. There is a significant amount of extrapolation involved in this procedure; for example, referring to Figs. 3(b) and 2 [which shows part of the time trace with which the potential of Fig. 3(b) was constructed] the potential is determined experimentally for $19<h<29$ nm, whereas the position of the closed state is $h_c \approx 14$ nm in this case. However, we have already shown in [28] that this extrapolation yields reliable values for the force up to considerably higher forces (~40 pN) than are measured here.

Higher tension leads to faster opening rates. With an external force, one approach [29,17] is to calculate the opening rate for escaping over a barrier, with the barrier height reduced by the work W done by the external force in pulling the particle over the barrier:

$$r(W) = r_0 e^{-(E-W)/T} = r(0)e^{W/T}, \tag{1}$$

where E is the unperturbed barrier height, $W=\phi(x_c)-\phi(x_c+s)$ is the work done by the external force field, $r(0)$ is the opening rate at zero external force (as measured in ensemble experiments), and T is the temperature in energy units. For a uniform external force F, $W=F\times s$ and the opening rate depends exponentially on the applied force:

$$r(F) = r(0)e^{F\times s/T}. \tag{2}$$

Figure 2(b) shows a plot of $\log r$ vs F_{closed} defined above; from the slope of the linear fit, using Eq. (2), we find for $r(0)$ and s, $r(0)=(1.16\pm0.14)\times10^{-1}$ s^{-1}, $s=0.47\pm0.06$ nm. An analysis which takes into account the nonuniformity of the force is presented in the next section; however, the results for the parameters $r(0)$ and s are the same within the error bars.

We performed the same measurements for a second hairpin (H_{GC}), which differs from the first (H_{AT}) only by the substitution of one GC pair in the stem with an AT pair (Fig. 1), obtaining the values $r(0)=(2.08\pm0.52)\times10^{-2}$ s^{-1}, $s=0.58\pm0.04$ nm. The zero-force rates differ by a factor of 6, which is consistent with the free energy difference corresponding to the substitution GC→AT (if we assume that the barrier height scales roughly with the free energy difference: for the free energy landscape of a "zipper" it is not unreasonable to assume that the effective barrier—i.e., the free energy difference between reactant and transition states—scales approximately with the length of the zipper and thus with the free energy difference between reactant and final states); however, the length scale s is the same in the two cases. For comparison, the experiment [10] at constant pulling rate for 15-bp-long duplexes finds $s\approx1.9$ nm, while the constant-force experiment [11] finds, for hairpins with 10-bp-long stems, $s\approx5$ nm.

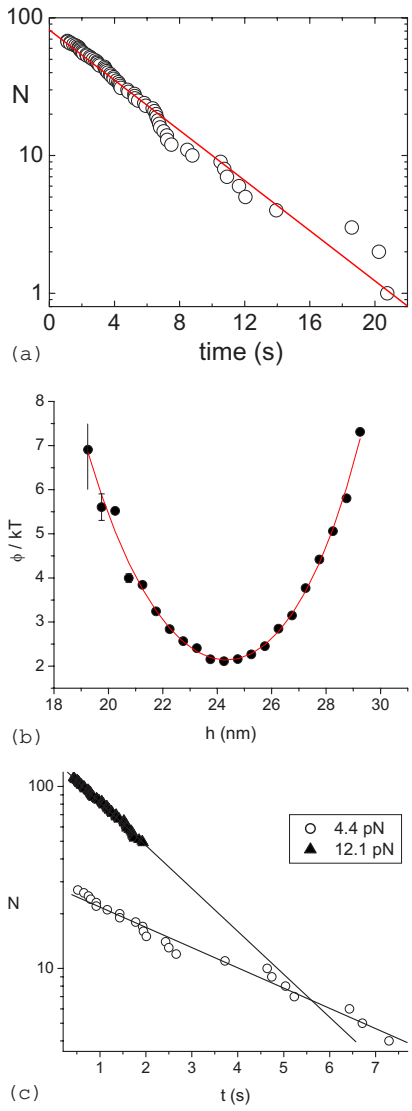

FIG. 3. (Color online) (a) The cumulative distribution of the duration of the closed state Δ obtained from a time trace such as shown in Fig. 2(a). With a total of $N(0)$ observed closing events, $N(0)-N(t)$ is the number of time intervals with $\Delta<t$. The slope in a semilogarithmic plot gives the opening rate of the hairpin [$(3.22\pm0.24)\times10^{-1}$ s^{-1} in this case]. The straight line is a linear fit. (b) The bead-slide interaction potential measured from the thermal motion of the bead with the hairpin in the open state. The solid line is a fit using Eq. (3). This potential was obtained from the time series of which Fig. 2(a) shows a part. The horizontal error bars on the experimental points (not shown) are the size of the bins (0.5 pN); the vertical error bars are determined from the number of counts in the histogram of the bead's position (not shown); for $\phi/kT<4$ these error bars are smaller than the points and so are not shown. When the DNA hairpin loop is closed, shortening of the molecular tether pulls the bead up the repulsive part of the potential, increasing the tension on the tether. (c) Different tensions in the DNA give rise to different opening rates. The plot shows the cumulative distribution of the residence time in the closed state, for two different experiments corresponding to measured tensions in the closed state of 4.4 and 12.1 pN. The slopes give opening rates of 1.87×10^{-1} and 4.67×10^{-1} s^{-1}, respectively.

B. Analysis of the force dependence of the rates

To measure the opening rate, we identify on the time trace the dwelling times Δ_i $(i=1,2,\ldots,N)$ in the closed state [Fig. 2(a)]. With a total of $N(0)$ observed closing events, $N(0)-N(t)$ is the number of time intervals with $\Delta<t$. We then plot the number of dwelling times $\Delta<t$, $N(t)$, vs t. In a semilogarithmic [Fig. 3(a)], the data follow a straight line and the slope is the opening rate. To measure the force field, we construct the potential energy ϕ of the bead-slide interaction from the thermal motion of the bead in the open state: from the time trace we obtain the probability $p(h)$ that the bead is at position h; this is related to the potential by the Boltzmann factor: $p(h) \propto \exp[-\phi(h)/kT]$ where T is the temperature. In Fig. 3(b) we show a measured bead-slide interaction potential. When the hairpin is closed, the shortening of DNA pulls the bead closer to the surface, up the repulsive part of the potential; the derivative of the potential at the equilibrium position x_c of the closed state ($h=x_c \approx 14$ nm for the trace of Fig. 2) gives the force on the DNA. We have shown previously [28] that this method gives accurate measurements of the force on the molecular tether. The interaction potential shown in Fig. 3(b) results from the sum of the electrostatic and entropic repulsion caused by the charged polymers attached to the surfaces and the restoring elastic force due to the DNA tether. Since both the electrostatic and entropic repulsion [30], as well as the tether elasticity [31], are roughly exponential with distance, we use the sum of two exponentials to fit the experimental potentials [Fig. 3(b)]:

$$\phi = Ae^{-k_1 h} + Be^{k_2 h} = \phi_E + \phi_T. \tag{3}$$

Physically, the first term represents the electrostatic and entropic repulsion between the surfaces, the second term the tether restoring force. In reality the distance dependence of the entropic repulsion term (as well as the tether restoring force) is more complicated, but the exponential is a reasonable heuristic approximation (see, e.g., [32]).

The tension F_{closed} on the hairpin in the closed state ($h=h_c$) is then

$$F_{closed} = \frac{\partial}{\partial h} Ae^{-k_1 h}\bigg|_{h=x_c} = \frac{\partial \phi_E}{\partial h}\bigg|_{h=x_c}. \tag{4}$$

Formula (3), while physically motivated, is just a fitting function which does not represent a unique decomposition of the measured potential ϕ. However, for $h \approx x_c$, $(\partial\phi_E/\partial h) \gg (\partial\phi_T/\partial h)$ so that in practice there is little difference between using $(\partial\phi_E/\partial h)|_{h=xc}$ or simply $(\partial\phi/\partial h)|_{h=xc}$ for the force in the closed state. Figure 3(c) shows that higher tensions lead to faster opening rates. In the presence of an external force, the opening rate $r(w)$ is given by

$$r(w) = r(0)e^{w/T}, \tag{5}$$

where $r(0)$ is the opening rate at zero external force and w is the work done by the external force in pulling the particle over the barrier which confines the closed state. For a uniform external force, $w=F\times s$, where the characteristic length scale s represents the position in the energy landscape of the top of the barrier. In this case, $r(F)=r(0)\exp(F\times s/T)$. However, in our experiment the external force is not constant in space and the work is really

$$w = \phi(x_c) - \phi(x_c + s), \tag{6}$$

where ϕ is the potential [Fig. 3(b)] and x_c the position of the closed state [e.g., $x_c \approx 14$ nm for the data of Fig. 2(a)]. Since we do know the potential $\phi(h)$, the length scale s can be obtained, in the framework of Eq. (5), by the following procedure [4]. We choose a value for s, and for each experiment we calculate $w(s)$ from the measured potential ϕ, using Eq. (6). We form the quantity $r(0)=r(w)\exp(-w/T)$, where $r(w)$ is the measured opening rate [see Eq. (5)]. This quantity should be the same for all experiments [i.e., independent of the force field, if Eq. (5) holds], so we vary s to find the value which best accomplishes this. Figure 4(a) shows, for the hairpin H_{AT}, the corresponding values $r(0)$ for three different choices of s; from this analysis we conclude $s \approx 0.53\pm0.04$ nm and $r(0) \approx (1.22\pm0.16)\times10^{-1}$ s^{-1} for the opening rate at zero force; Fig. 4(b) shows the same analysis for the hairpin H_{GC}, giving $s \approx 0.58\pm0.04$ nm and $r(0) \approx (2.08\pm0.52)\times10^{-2}$ s^{-1}. These values are within error bars of those obtained from the analysis for constant force according to Eq. (2), which basically uses a linearization of the potential around x_c.

C. Simulations of the PBD model

Comparing the different experiments is not straightforward because of the different sequences and conditions used; it is therefore useful to turn to a model, where one can change only one parameter or condition at a time. We invoke the well-established PBD model for double-stranded DNA [18]. It has been previously shown that this model not only successfully reproduces details of the thermal denaturation transition of double-stranded DNA [19,20], but it can also, through the use of Monte Carlo (MC) simulations, provide significant insight on the mechanical unzipping of double-stranded DNA [21].

The potential energy of the model reads

$$V(y) = \sum_n \left[D_n(e^{-a_n y_n} - 1)^2 + \frac{k}{2}(1 + \rho e^{-\beta(y_n + y_{n+1})})(y_n - y_{n-1})^2 \right],$$

where the sum is over all the base pairs of molecule and y_n denotes the relative displacement from equilibrium at the nth base pair. The first term of the potential energy is a Morse potential that phenomenologically represents the hydrogen bonds between the bases. The second term is a nearest-neighbor coupling representing the stacking interaction between adjacent base pairs: it comprises a harmonic coupling multiplied by a term that strengthens the coupling when the molecule is closed and makes it weaker when its strands are separated, in this way taking into account the different stiffness (i.e., entropic effects) of DNA double and single strands. This nonlinear coupling results in long-range cooperative effects in the denaturation, leading to an abrupt entropy-driven transition [18]. A more accurate description of the stacking interaction [33] requires consideration of the ten different possible combinations of neighboring bases.

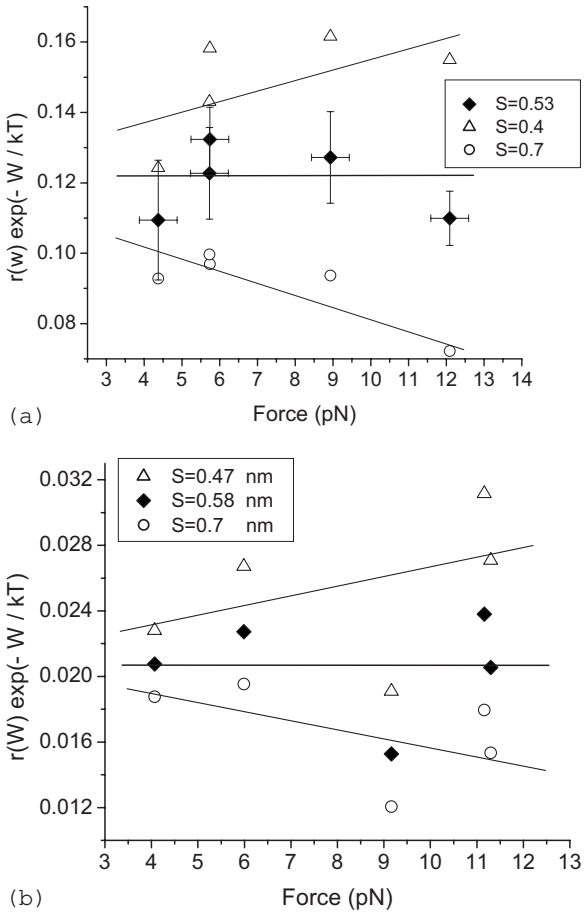

FIG. 4. (a) For the hairpin H_{AT}, the quantity $r(0)=r(w)\exp[-w(s)/T]$, vs the mechanical tension in the closed state, $F=(\partial\phi\partial h)(x_c)$, for different choices of the parameter s. $r(w)$ is the measured opening rate, $w(s)=\phi(x_c)-\phi(x_c+s)$ is the work performed by the external force in opening the bond, ϕ is the measured potential energy surface, and x_c is the position of the closed state. The correct choice of s should result in $r(0)$ (the opening rate at zero force) being the same for all measurements. The figure shows that if s is chosen too small, there is a systematic increase of $r(0)$ for increasing F, while if s is too large, there is a systematic decrease. The solid lines are best linear fits through the data plotted for different s. In this manner we determine $s\approx 0.53\pm 0.04$ nm and $r(0)\approx(1.22\pm 0.16)\times 10^{-1}$ s^{-1}. (b) Same analysis as in (a), for the hairpin H_{GC}. We obtain the values $s\approx 0.58\pm 0.04$ nm and $r(0)\approx(2.08\pm 0.52)\times 10^{-2}$ s^{-1}. The error bars for these data points are similar to the ones in (a).

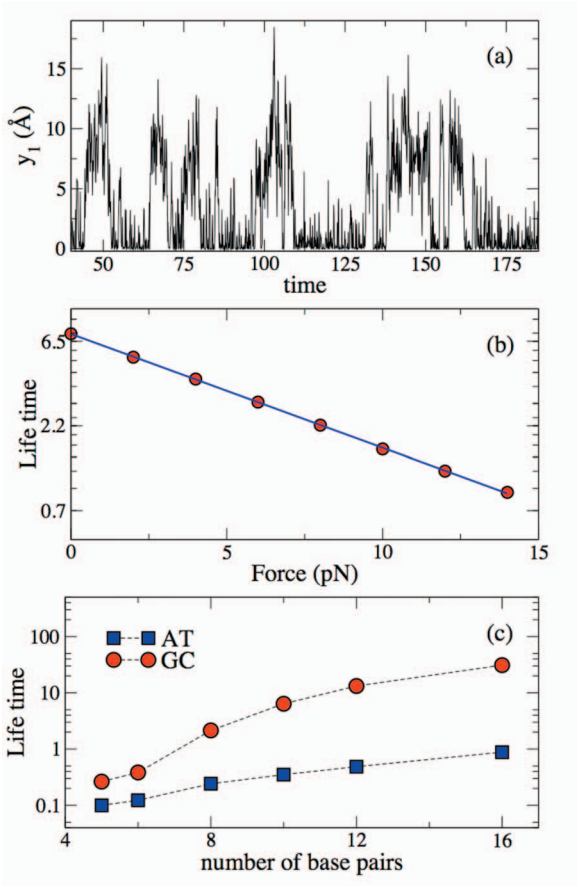

FIG. 5. (Color online) Results from the simulation of the Peyrard-Bishop-Dauxois model. (a) The base-to-base distance in the course of time (MC steps $\times$ 1000) for the first base pair of H_{AT}, at constant force. (b) Semilogarithmic plot of the lifetime of the closed state vs force, for H_{AT}, from the simulation. From the linear fit we extract $s=0.58$ nm. (c) The zero force lifetime of the closed state, $1/r(0)$, for homogeneous AT and GC sequences as a function of the number of base pairs.

Rather than applying ten additional parameters we opt for simplicity and use a single parameter such that only the pairing interaction depend on the sequence here. This is achieved by giving different values to the parameters of the Morse potential, depending on the base-pair type of the site considered: AT or GC. The parameter values we have used are those used in Ref. [19]: $k=0.025$ eV/Å^2, $\rho=2$, and $\beta=0.35$ Å^{-1} for the intersite coupling, while for the Morse potential $D_{GC}=0.075$ eV and $a_{GC}=6.9$ Å^{-1} for a GC base pair and $D_{AT}=0.05$ eV and $a_{GC}=4.2$ Å^{-1} for a AT base pair. These parameters were chosen to fit thermodynamics properties of DNA [14]. One should be cautious in relating these parameters directly to microscopic properties, but recall that they arise as a result of several physical phenomena at the microscopic level.

Here we slightly modify this model to apply to DNA hairpins by adding a square potential at the terminal base pair so that the DNA double strand is incapable of complete denaturation (i.e., the square potential models the effect of the loop of the hairpin). The constant force is then applied at the opposite end of the DNA double strand. It is important to note that we do not fit any parameters of the model in order to produce the following results; we use precisely the parameters established to reproduce the melting transition of short DNA sequences [19]. In Fig. 5(a) we show what corresponds to the bead position versus Monte Carlo steps (which is analogous to time) [34]. We clearly observe a behavior similar to what is observed experimentally: namely, a repeated switching between the open and closed states of the hairpin. Similarly to the experiments we can for each event measure the duration of the closed state in terms of Monte Carlo steps, and we can thus obtain the lifetime of the closed state for any applied force. In Fig. 5(b) we plot this lifetime versus

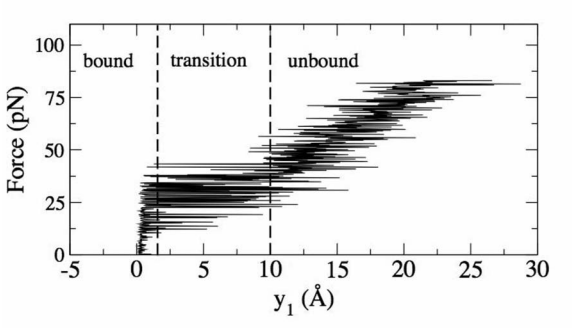

FIG. 6. Force (proportional to MC time) vs displacement for the first bp of H_{AT} from the simulation at constant pulling rate.

the applied force F, for the H_{AT} sequence. We find that the behavior is exactly as given by Eq. (2), with $s=0.58$ nm. For the H_{GC} hairpins we find a similar result, again with $s=0.58$ nm. The sequence and length dependence of $r(0)$ obtained from the model is reported in Fig. 5(c), which shows the lifetime of the close state of pure AT and GC s hairpins of variable length. We observe the closed state of the 10-bp GC hairpin to have a roughly 30 times longer lifetime than the AT hairpin. This yields a factor of 3 difference in lifetime per base pair, which is consistent with the experimental result regarding the zero force rate of the H_{AT} and H_{GC} sequences.

Mechanical unzipping at constant loading rate provides a different way of exploring hairpin dynamics. We have performed constant rate simulations (Fig. 6) [21] on the sequence $TTGAAATACCGACCG(AT)_{50}$ [10,35], collected the rupture force distributions (shown in Fig. 7), and fitted with the theoretical distribution [23], as in [10], to extract s.

We find $s=1.2$ nm, independently of the loading rate, in good agreement with the experiments in [10]. However, the s provided by the constant-force analysis of the simulation for the same sequence [10] is quite different: $s=0.56$ nm. Thus the apparent position of the transition state is different in the two cases.

III. MATERIALS AND METHODS

A. Sample preparation

Flow cells were built from microscope slides and cover slips, separated by 75-μ plastic spacers, as described before [26]. The Piranha-cleaned slides were stored in deionized water and used within a week. The DNA molecule which tethers the bead to the slide consists of the 40-bases-long DNA hairpin (20 bases loop+10 bp stem) and a 17-bases-long tail on both ends. This molecule is attached to the slide and bead through adapter DNA 18mers, with 17-base complementarity to the tails of the probe DNA (Fig. 1). The adapters are themselves grafted to the surfaces through biotin-avidin couplings. The surface of the flow cell was functionalized as follows. A 20:1 mixture of BSA and biotinilated BSA (Sigma), 10 mg/mL in filtered PBS 140 mM, pH=7.4, where the biotinilated BSA concentration is 0.5 mg/ml (this buffer was used throughout the experiment) was incubated in the flow cell for 5 h. The cell was washed

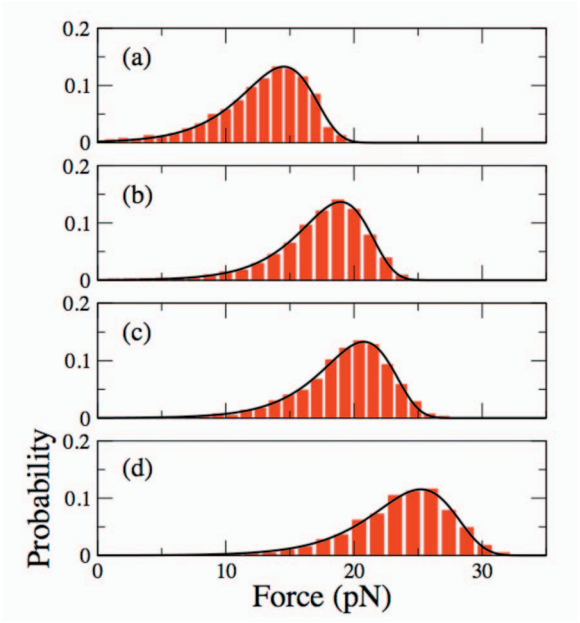

FIG. 7. (Color online) Rupture force distributions for the sequence used in [10] for four different loading rates k_0: (a) $k_0=5r_0$, (b) $k_0=25r_0$, (c) $k_0=2.5\times10^2 r_0$, and (d) $k_0=2.5\times10^3 r_0$, where $r_0=10^{-8}$ pN/MC steps. Fitting the theoretical distribution of the single bond dissociation [23] to the numerical data we find both s and zero-force opening rate are independent of k_0.

twice with PBS to remove free BSA and a second layer of Streptavidin (Sigma) 0.5 mg/ml was incubated for 3 h. After washing, we incubate overnight a mixture of dummy, adapter, and probe oligomers in the ratio 500:1, total concentration of probe oligomers 0.4 mol/μL. The dummy and adapter oligomers are biotinilated at one end; all oligomers were from Operon Technologies, CA. The purpose of the dummy 15mer on the surfaces is to provide a charged polymer layer which prevents the bead from sticking to the slide (Fig. 1). The low surface concentration of adapters favors a single tether configuration when the bead binds. The DNA tether contains the 40 bases hairpin:

5′ - GTACTGCGTGATTCTAGTGTG

TATCTGGCGCACGCAGTAC - 3′.

The complete sequence of the tether is

5′ - GCGGCACCTCCGCTGTTGTACTGC

GTGATTCTAGTGTGTATCTGGCGCACG

CAGTACCTCTCGACGGCGACCGC - 3′.

The sequences of the other oligomers are
adapter (on the slide):

biotin - TTTGCGGTCGCCGTCGAG - 5′

adapter (on the bead):

5′ - CAGCGGAGGTGCCGCTTT - biotin

dummy:

biotin - GACTGTTCGGGTAAA - 3′.

Here 1-μm-diam Streptavidin functionalized beads (Bangs Laboratories) were washed with a solution of PBS and 0.005% Tween-20 and incubated overnight with adapter oligomers (10^8 beads and 15 pmol adapter DNA in 50 μl PBS). After a final wash with PBS and Tween-20, the beads were stored at 4 °C and used within 2 weeks.

B. Optical setup

The evanescent wave at the bottom of the flow cell is produced by total internal reflection (at the slide-solution interface) of a parallel light beam from a 20-mW He-Ne laser, steered by a dove prism coupled to the flow cell with immersion oil [Fig. 1(a)]. The evanescent field decays exponentially into the flow cell, with a penetration depth $\delta \approx 86$ nm. A bead in close proximity with the interface scatters some light, the scattered intensity providing a measure of the distance of the bead to the interface, according to $I = I_c \exp(-h/\delta)$, where I is the scattered intensity, I_c the intensity at contact, h the separation between the bead and the surface, and δ the penetration depth [36,27]. Relative changes in the position of the bead can be measured from $\Delta h = h_2 - h_1 = \delta \ln (I_2/I_1)$. The absolute position h can be obtained if the contact intensity I_c is known; this can be measured by collapsing the bead on the surface at the end of the experiment. We have calibrated the distance measurements [36,37] by using the observed thermal motion of free beads to obtain the force acting on the bead (as explained below); far from the surface, this force is the bead's weight.

Light scattered by the polystyrene beads is collected through a microscope objective (Zeiss 63X, NA=0.8) and focused on a photodiode. The signal is recovered through lock-in detection and acquired with a computer.

C. Experimental procedure

A dilute suspension of functionalized beads is introduced in the functionalized flow cell, and within about 1 h some beads tether to the probe DNA on the surface and are visible in the evanescent field. A single bead is brought into the field of view of the photodiode and its thermal fluctuations are monitored for some 30 min. The amplitude of the bead's fluctuations and its response to small flows indicate with high probability whether the bead is held by one or more molecular tethers [28]. Namely, beads attached through multiple tethers (which are rare in the samples because of the low surface density of attachment points used) show distinctively smaller amplitudes of their thermal motion and complicated multiple states characterized by more than two levels of bead-slide separation in the signal. In control experiments where the DNA tether did not contain the self-complementary sequence of the hairpin's stem, we did not observe the "telegraph signal" of Fig. 2(a).

IV. CONCLUSIONS

We contribute a set of measurements of hairpin dynamics under nonhomogeneous force fields. Comparing with previous experiments and using the PBD model to simulate constant-force and constant-pulling-rate experiments explicitly shows that the apparent position of the transition state as measured by the parameter s is in general different for different force fields and different experimental conditions. As a general remark, with an extended surface of contact, different boundary conditions (e.g., constant force, constant rate, zero force) may force different pathways for opening the bond, leading to different rates and different rate dependences on the force. The recently published comprehensive study of 20 different hairpins [11] where the force field is homogeneous in space and constant in time finds the transition state generally located 1–2 bp away from the open state. The reason is that the conditions of the latter experiment—constant force close to the value for which the open and closed states are equally likely—force the hairpin to open by progressively unzipping from one end to the other, while the sum of a roughly linear "zipper" energy landscape and a linear external potential produces a free energy landscape with a maximum close to the open state [11]. Thus for relatively long stems the situation is clear. For short stems, different opening pathways may contribute significantly—for example, thermal fraying of the opposite end of the hairpin. In this case, the measured value of s may no longer represent essentially the stem length and may also be more sensitive to the detailed conditions of the experiment. In general, the free energy landscape $\mathcal{G}(x) = E(x) + \phi(x) - TS(x)$ where x is the distance of the two ends of the hairpin, E the bond energy of the bases, ϕ the external potential, and S the entropy of the extended ss-DNA, depends on the force field ϕ, so that different external potentials ϕ may give rise to different apparent transition states. This has also been recently demonstrated in mechanical unfolding experiments of a protein domain [38]. To roughly summarize the situation for short stems, in the present experiment the measured s corresponds to the beginning of the stem ($s=0.6$ nm for a 10-bp stem); in [11], the measured s corresponds to the end of the stem ($s=5$ nm for a 10-bp stem), and in [10], they find a value in between ($s=1.9$ nm for a 15-bp stem). If we trust the result from the PBD model, redoing the experiment [10] at constant force, without changing anything else, would result in a smaller s; this would make the result from [10], also in view of the different stem lengths, comparable to the result of the present experiment. The discrepancy with [11] is unexplained but could result from the different sequences and experimental conditions.

ACKNOWLEDGMENTS

We thank Steven Koch for discussions. This work was supported by NSF Grant No. DMR-0405632. Work at Los Alamos is supported by the U.S. Department of Energy.

[1] R. P. Merkle *et al.*, Nature (London) **397**, 50 (1999).
[2] E. Evans, A. Leung, D. Hammer, and S. Simon, Proc. Natl. Acad. Sci. U.S.A. **98**, 3784 (2001).
[3] S. J. Koch and M. Wang, Phys. Rev. Lett. **91**, 028103 (2003).
[4] S. Dixit, M. Singh-Zocchi, J. Hanne, and G. Zocchi, Phys. Rev. Lett. **94**, 118101 (2005).
[5] J. Liphardt, B. Onoa, S. B. Smith, I. Tinoco, Jr., and C. Bustamante, Science **292**, 733 (2001).
[6] P. T. X. Li, D. Collin, S. B. Smith, C. Bustamante, and I. Tinoco, Jr., Biophys. J. **90**, 250 (2006).
[7] T. Strunz, K. Oroszlan, R. Schafer, and H.-J. Guntherodt, Proc. Natl. Acad. Sci. U.S.A. **96**, 11277 (1999).
[8] U. Bockelmann, B. Essevaz-Roulet, and F. Heslot, Phys. Rev. Lett. **79**, 4489 (1997).
[9] U. Bockelmann, P. Thomen, and F. Heslot, Biophys. J. **87**, 3388 (2004).
[10] M. J. Lang, P. M. Fordyce, A. M. Engh, K. C. Neuman, and S. M. Block, Nat. Methods **1**, 133 (2004).
[11] M. T. Woodside, W. M. Behnke-Parks, K. Larizadeh, K. Travers, D. Herschlag, and S. M. Block, Proc. Natl. Acad. Sci. U.S.A. **103**, 6190 (2006).
[12] M. Craig, D. Crothers, and P. Doty, J. Mol. Biol. **62**, 383 (1971).
[13] D. Pörschke, Biophys. Chem. **2**, 97 (1974).
[14] G. Bonnet, O. Krichevsky, and A. Libchaber, Proc. Natl. Acad. Sci. U.S.A. **95**, 8602 (1998).
[15] A. Ansari, S. Kuznetsov, and Y. Shen, Proc. Natl. Acad. Sci. U.S.A. **98**, 7771 (2001).
[16] J. R. Grunwell, J. L. Glass, T. D. Lacoste, A. A. Deniz, D. S. Chemla, and P. G. Schultz, J. Am. Chem. Soc. **123**, 4295 (2001).
[17] E. Evans, Faraday Discuss. **111**, 1 (1999).
[18] T. Dauxois, M. Peyrard, and A. R. Bishop, Phys. Rev. E **47**, R44 (1993).
[19] A. Campa and A. Giansanti, Phys. Rev. E **58**, 3585 (1998).
[20] S. Ares, N. K. Voulgarakis, K. Ø. Rasmussen, and A. R. Bishop, Phys. Rev. Lett. **94**, 035504 (2005).
[21] N. K. Voulgarakis, A. Redondo, A. R. Bishop, and K. Ø. Rasmussen, Phys. Rev. Lett. **96**, 248101 (2006); N. K. Voulgarakis, A. Redondo, A. R. Bishop, and K. Ø. Rasmussen, Nano Lett. **6**, 1483 (2006); N. K. Voulgarakis, G. Kalosakas, K. Ø. Rasmussen, and A. R. Bishop, *ibid.* **4**, 629 (2004).
[22] O. K. Dudko, G. Hummer, and A. Szabo, Phys. Rev. Lett. **96**, 108101 (2006).
[23] E. Evans, and K. Ritchie, Biophys. J. **72**, 1541 (1997).
[24] E. Evans, Annu. Rev. Biophys. Biomol. Struct. **30**, 105 (2001).
[25] S. Cocco, R. Monasson, and J. F. Marko, Phys. Rev. E **65**, 041907 (2002).
[26] M. Singh-Zocchi, S. Dixit, V. Ivanov, and G. Zocchi, Proc. Natl. Acad. Sci. U.S.A. **100**, 7605 (2003).
[27] H. Jensenius and G. Zocchi, Phys. Rev. Lett. **79**, 5030 (1997).
[28] G. Zocchi, Biophys. J. **81**, 2946 (2001).
[29] H. A. Kramers, Physica (Utrecht) **7**, 284 (1940).
[30] J. Israelachvili, *Intermolecular and Surface Forces* (Academic, London, 1991).
[31] M. N. Dessinges, B. Maier, Y. Zhang, M. Peliti, D. Bensimon, and V. Croquette, Phys. Rev. Lett. **89**, 248102 (2002).
[32] W. B. Russel, D. A. Saville, and W. R. Schwalter, *Colloidal Dispersions* (Cambridge University Press, Cambridge, England, 1991).
[33] P. Yakovchuk, E. Protozanova, and M. D. Frank-Kamenetskii, Nucleic Acids Res. **34**, 564 (2006).
[34] It is important to notice that because of the rescaled nature of the model ($y_1=0$ for a closed hairpin) the scales in Figs. 2(a) and 5(a) are not directly comparable. This gives the artificial impression that both the close and open states are less well defined in the model. A closer inspection reveals that in fact this is not the case.
[35] We have added 50 AT base pairs at the end of the sequence used in [10] to avoid boundaries effects of PBD model [20].
[36] D. C. Prieve and N. A. Frej, Langmuir **6**, 396 (1990).
[37] M. Singh-Zocchi, J. Hanne, and G. Zocchi, Biophys. J. **83**, 2211 (2002).
[38] M. Schlierf and M. Rief, Biophys. J. **90**, L33 (2006).